Generalized FDTD-ADI: An Unconditionally Stable Full-Wave Maxwell's Equations Solver for VLSI Interconnect Modeling

Charlie C.-P. Chen, Tae-Woo Lee, Narayanan Murugesan, and Susan C. Hagness

Department of Electrical and Computer Engineering
University of Wisconsin-Madison
1415 Engineering Drive, Madison, WI 53706
(e-mail: chen@engr.wisc.edu, hagness@engr.wisc.edu)

Abstract—**The finite-difference time-domain (FDTD) method of solving the full-wave Maxwell's equations has been recently extended to provide accurate and numerically stable operation for time steps exceeding the Courant limit. The elimination of an upper bound on the size of the time step was achieved using an alternating-implicit direction (ADI) time-stepping scheme. This greatly increases the computational efficiency of the FDTD method for classes of problems where the cell size of the three-dimensional space lattice is constrained to be much smaller than the shortest wavelength in the source spectrum. One such class of problems is the analysis of high-speed VLSI interconnects where full-wave methods are often needed for the accurate analysis of parasitic electromagnetic wave phenomena. In this paper, we present an enhanced FDTD-ADI formulation which permits the modeling of realistic lossy materials such as semiconductor substrates and metal conductors as well as artificial lossy materials needed for perfectly matched layer (PML) absorbing boundary conditions. Simulations using our generalized FDTD-ADI formulation are presented to demonstrate the accuracy and extent to which the computational burden is reduced by the ADI scheme.**

I. Introduction

RECENT advances in VLSI technology have resulted in higher clock rates and low-pass signal bandwidths that extend well into the microwave frequency range. At these high speeds, electromagnetic wave propagation and radiation effects become significant and consequently limit the performance of on-chip and off-chip VLSI interconnects. For example, at 10 GHz, a 5-mm-long interconnect may in fact radiate much like an antenna since its length corresponds to a substantial fraction of a wavelength. Quasi-static analysis techniques, such as capacitance and inductance extraction using method of moments [1], [2], [3] and model order reduction using the partial element equivalent circuit method [4], work extremely well at lower frequencies, but may have limited applicability in this regime. To accurately analyze parasitic electromagnetic wave phenomena at these higher frequencies, vectorial Maxwell's equations modeling tools are needed.

As computing resources have become more powerful, full-wave methods such as the method of moments, the finite element method, and the finite-difference time-domain (FDTD) method have become extremely versatile tools for solving electromagnetic wave problems. In particular, the accuracy, efficiency, and overall utility of FDTD has been demonstrated in recent years for a variety of complex high-speed interconnect design problems related to EMI/EMC, signal integrity, and packaging (for example, see [5], [6], [7], [8], [9]). Furthermore, numerous extensions and enhancements to FDTD have been developed, which further broaden its appeal, improve its computational efficiency, and augment its capability [10].

However, there remains a class of VLSI interconnect problems for which FDTD modeling persists to be very computationally intensive. These difficulties, which are reviewed in Section II in the context of a brief summary of the fundamental features of the FDTD method, may be alleviated by a recently proposed alternating-direction implicit (ADI) time-stepping scheme [11], [12]. The original 3-D FDTD-ADI formulation reported in [12] solves a simplified version of Maxwell's curl equations where the electric and magnetic conduction currents are assumed to be zero. In Sections III and IV, we present an important extension to the FDTD-ADI formulation that includes the contributions from the conduction currents. The need for this extension is two-fold. First, we are interested in modeling VLSI interconnects where the lossy nature of realistic insulators, semiconductors, and conductors should be accounted for. Second, the creation of perfectly matched layer (PML) absorbing boundary conditions (ABCs) [13] is necessary to simulate open regions using a truncated computational domain. The PML formulation requires the simulation of lossy regions near the grid boundaries. Simulation results presented in Section V demonstrate the accuracy and extent to which the computational burden is reduced by the ADI scheme.

II. Numerical Accuracy and Stability of the FDTD Method

The FDTD method [14] is a computationally efficient approach for modeling sinusoidal or impulsive electromagnetic wave interactions with arbitrary three-dimensional structures. It is an explicit

The work of C.-P. Chen and N. Murugesan was supported by the Avant! Corp. and the Intel Corp. The work of S. C. Hagness and T.-W. Lee was supported by NSF Faculty Early Career Development Award ECS-9985004. Computing resources were provided by Cray, Inc.

grid-based technique for the direct solution of the fundamental Maxwell's curl equations, shown below for the six components of the electric and magnetic field vectors, $\vec{E}$ (volts/meter) and $\vec{H}$ (amperes/meter):

$$\varepsilon\frac{\partial E_x}{\partial t}+\sigma E_x = \frac{\partial H_z}{\partial y}-\frac{\partial H_y}{\partial z} \quad (1)$$

$$\varepsilon\frac{\partial E_y}{\partial t}+\sigma E_y = \frac{\partial H_x}{\partial z}-\frac{\partial H_z}{\partial x} \quad (2)$$

$$\varepsilon\frac{\partial E_z}{\partial t}+\sigma E_z = \frac{\partial H_y}{\partial x}-\frac{\partial H_x}{\partial y} \quad (3)$$

$$\mu\frac{\partial H_x}{\partial t}+\sigma^\star H_x = \frac{\partial E_y}{\partial z}-\frac{\partial E_z}{\partial y} \quad (4)$$

$$\mu\frac{\partial H_y}{\partial t}+\sigma^\star H_y = \frac{\partial E_z}{\partial x}-\frac{\partial E_x}{\partial z} \quad (5)$$

$$\mu\frac{\partial H_z}{\partial t}+\sigma^\star H_z = \frac{\partial E_x}{\partial y}-\frac{\partial E_y}{\partial x} \quad (6)$$

Here, σ and $\sigma^\star$ are the electric conductivity (S/m) and equivalent magnetic loss (ohms/m), respectively.

In the standard formulation, the spatial derivatives are implemented using central finite differences on staggered Cartesian grids for the electric and magnetic fields. Central finite differences are also used to approximate the temporal derivatives, resulting in an explicit leapfrog integration scheme that marches the discretized electric and magnetic fields forward in time. The explicit time-stepping expressions and their derivation have been documented extensively elsewhere [14], so they will not be repeated here. Figure 1 summarizes the explicit time-stepping nature of the standard algorithm. The notation $V|^n_{i,j,k}$ is used throughout this paper to represent vector field component V sampled at time $n\Delta t$ and space coordinates $(i\Delta x, j\Delta y, k\Delta z)$, where Δt is the time step and Δx, Δy, and Δz are the space increments. Note that the electric and magnetic fields are staggered in time by $\Delta t/2$.

To minimize numerical dispersion errors and thereby ensure numerical accuracy, the space and time increments must be no larger than a small fraction of the smallest wavelength and temporal period of interest. Typically, 10 to 20 samples per cycle (spatial wavelength $\lambda_{\min}$, and temporal period $T_{\min}$) provide sufficient accuracy. The numerical stability of the standard algorithm further requires a bounding of the time step relative to the space increment. This Courant stability bound is given in three dimensions [14] by

$$\Delta t \le \frac{1}{c\sqrt{\frac{1}{(\Delta x)^2}+\frac{1}{(\Delta y)^2}+\frac{1}{(\Delta z)^2}}}. \quad (7)$$

where c is the speed of wave propagation in free space. For a computational domain comprised of cubic grid cells of space increment Δ, this stability limit simplifies to $\Delta t \le \Delta/(c\sqrt{3})$.

Most commonly, the minimum geometrical feature size, b, of the structure to be modeled is much larger than the needed grid cell size, Δ, for the given frequency range of interest. In this case, the grid resolution is chosen such that the wave is spatially sampled at a rate of N points per smallest wavelength ($\Delta = \lambda_{\min}/N$), and the minimum feature size is modeled using b/Δ grid cells. The upper bound on the time step dictated by the stability limit ($\Delta t|_{max} = T_{\min}/(N\sqrt{3})$) is comparable to the desired time step based on numerical accuracy considerations ($\Delta t|_{max} = T_{\min}/N$); that is, if the stability limit didn't exist, the choice of the time step would not change much because of the need to adequately sample the temporal waveform. It is this common scenario for which the FDTD algorithm is extremely computationally efficient. Typically, no more than 1,000 time steps are required to complete a simulation.

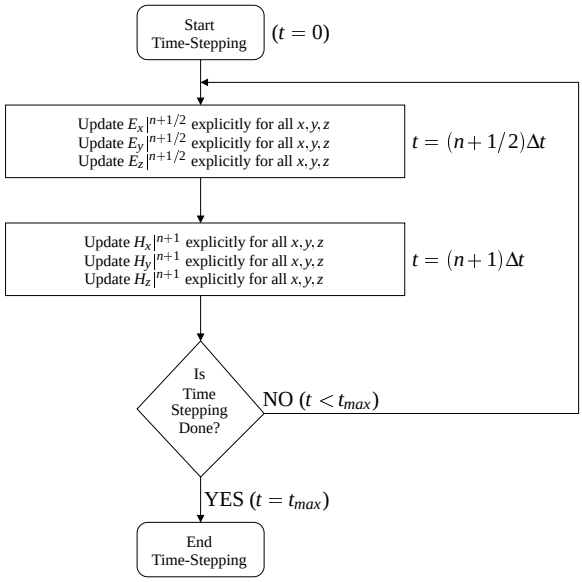

Fig. 1. Flowchart of the standard FDTD time-stepping process.

There is, however, a class of problems that does not fit this scenario. Consider a high-speed VLSI interconnect with a minimum geometrical feature size of 1 μm and a signal rise time less than 100 ps. The frequency spectrum of this signal extends to nearly 10 GHz. As a result, the minimum wavelength of interest is on the order of 3 cm in free space, or 1.5 cm in SiO_2 ($\varepsilon_r = 4$). Numerical accuracy considerations would then suggest that an appropriate grid cell size would be on the order of 1.0 mm (between 10 and 20 points per wavelength). However, to model the micron-scale features of the interconnect, the spatial increment must be on the order of 1.0 μm or less. As a result, the upper bound on the time step is approximately 2 fs. Simulating the 100-ps rise time of a digital signal alone would require 50,000 time steps! This example illustrates the scenario where the minimum geometrical feature size is much smaller than 1/10th or 1/20th of the smallest wavelength of interest. Consequently, the limit on Δt is orders of magnitude smaller than needed for numerical accuracy considerations, and a formidable number of time steps are required to complete the simulation.

The difficulty with this second scenario would be alleviated if the upper bound on Δt was not linked to Δ via a stability limit.

For example, if we could choose Δt to be 1 ps (which is still small enough to adequately sample the temporal period at a frequency of 10 GHz and thus maintain high accuracy) while keeping a spatial increment of 1 μm, then only 100 time steps would be required to march through the 100-ps rise time. This flexibility appears to be now available with the advent of an alternating-direction implicit (ADI) time-stepping scheme for FDTD [11], [12] which has been shown to be unconditionally stable.

III. Numerical Formulation of the Generalized FDTD-ADI Algorithm

Here we present the derivation of the generalized FDTD-ADI algorithm for the case of physical media only. In Section IV, this work is further extended to the case of both physical and artificial (PML) media. In both cases, the discretized vector field components are staggered in space, as in the conventional Yee grid, but collocated rather than staggered in time. Also, in contrast to the standard FDTD formulation which only requires one iteration to advance from the n^{th} to $(n+1)^{th}$ time step, the FDTD-ADI formulation requires one sub-iteration to advance from n to $n+1/2$ and a second sub-iteration to advance from $n+1/2$ to $n+1$. This process is illustrated in Figure 2. Due to limited space, we present the complete derivation of an implicit update expression for only the E_x field component and explicit update expressions for only the H_z and H_y field components. Using these sample derivations as a guide, it is straightforward to derive the implicit update expressions for E_y and E_z and the explicit update expression for H_x.

A. *Sub-Iteration 1: Advance the 6 field components from time step n to time step n + 1/2*

Step 1. We start by applying central differences to Eq. 1. In this first sub-iteration, every term is discretized using finite differences centered at $n+1/4$ as follows:

$$\varepsilon \left.\frac{\partial E_x}{\partial t}\right|^{n+1/4} + \sigma E_x|^{n+1/4} = \left.\frac{\partial H_z}{\partial y}\right|^{n+1/2} - \left.\frac{\partial H_y}{\partial z}\right|^{n} \tag{8}$$

Note that the spatial derivative terms involving magnetic fields are discretized at time steps $n+1/2$ and n, giving an overall center point of $n+1/4$. Upon substituting centered finite-difference approximations, we obtain the following expression:

$$\begin{aligned} & \varepsilon_{i+\frac{1}{2},j,k}\left(\frac{E_x|^{n+1/2}_{i+\frac{1}{2},j,k} - E_x|^{n}_{i+\frac{1}{2},j,k}}{\Delta t/2}\right) \\ + \quad & \sigma_{i+\frac{1}{2},j,k}\left(\frac{E_x|^{n+1/2}_{i+\frac{1}{2},j,k} + E_x|^{n}_{i+\frac{1}{2},j,k}}{2}\right) \\ = & \frac{H_z|^{n+1/2}_{i+\frac{1}{2},j+\frac{1}{2},k} - H_z|^{n+1/2}_{i+\frac{1}{2},j-\frac{1}{2},k}}{\Delta y} - \frac{H_y|^{n}_{i+\frac{1}{2},j,k+\frac{1}{2}} - H_y|^{n}_{i+\frac{1}{2},j,k-\frac{1}{2}}}{\Delta z} \end{aligned} \tag{9}$$

Here, we have used the conventional semi-implicit formulation to evaluate the conduction current density terms. All fields at time step n are known; the fields at time step $n+\frac{1}{2}$ are unknown. Note that in sub-iteration 1, the $\partial H_z/\partial y$ term is evaluated implicitly from as-yet unknown field data at time-step $n+1/2$, while the $\partial H_y/\partial z$ term is evaluated explicitly from known field data at time step n.

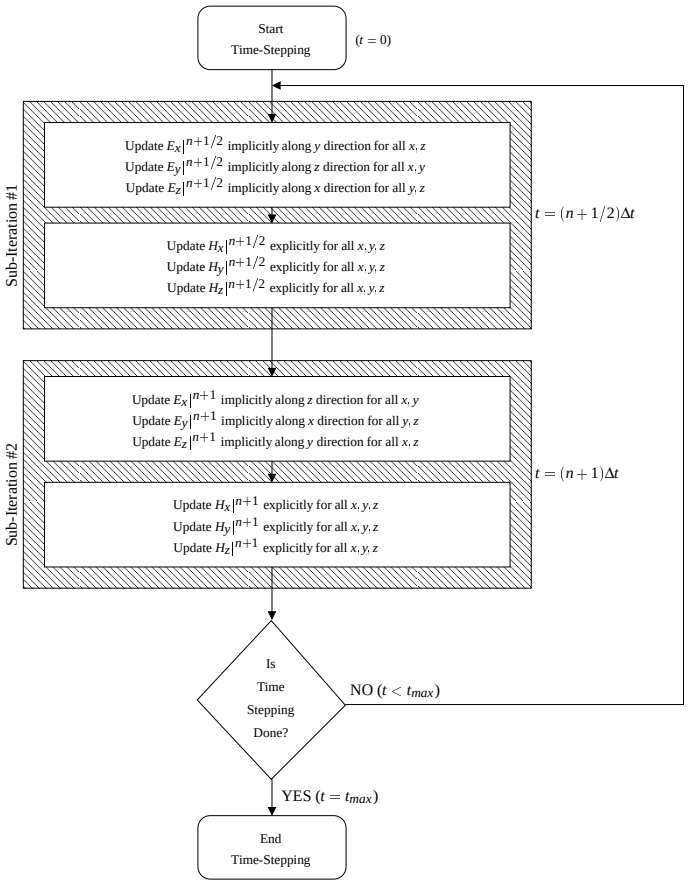

Fig. 2. Flowchart of the FDTD-ADI time-stepping process.

Step 2. Our aim is to find the value of the unknown E_x at time step $n+\frac{1}{2}$. However, there are also unknown values of H_z on the right hand side of Eq. (9). To eliminate the unknown terms, we apply finite-difference approximations centered at $n+1/4$ to Eq. (6) to obtain the following expression:

$$\begin{aligned} & \mu_{i+\frac{1}{2},j+\frac{1}{2},k}\left(\frac{H_z|^{n+1/2}_{i+\frac{1}{2},j+\frac{1}{2},k} - H_z|^{n}_{i+\frac{1}{2},j+\frac{1}{2},k}}{\Delta t/2}\right) \\ + \quad & \sigma^{\star}_{i+\frac{1}{2},j+\frac{1}{2},k}\left(\frac{H_z|^{n+1/2}_{i+\frac{1}{2},j+\frac{1}{2},k} + H_z|^{n}_{i+\frac{1}{2},j+\frac{1}{2},k}}{2}\right) \\ = \quad & \frac{E_x|^{n+1/2}_{i+\frac{1}{2},j+1,k} - E_x|^{n+1/2}_{i+\frac{1}{2},j,k}}{\Delta y} - \frac{E_y|^{n}_{i+1,j+\frac{1}{2},k} - E_y|^{n}_{i,j+\frac{1}{2},k}}{\Delta x} \end{aligned} \tag{10}$$

The two unknowns in this equation are also E_x and H_z at time step $n+\frac{1}{2}$.

Step 3. Finally, we use Eq. (10) to eliminate the unknown $H_z|^{n+\frac{1}{2}}$ terms in Eq. (9) and obtain the following expression for

the unknown E_x fields at the $n+1/2^{th}$ time step:

$$\begin{aligned} C_{a_{i+\frac{1}{2},j,k}} E_x|^{n+1/2}_{i+\frac{1}{2},j,k} - C_{b_{i+\frac{1}{2},j,k}} E_x|^{n+1/2}_{i+\frac{1}{2},j+1,k} - C_{c_{i+\frac{1}{2},j,k}} E_x|^{n+1/2}_{i+\frac{1}{2},j-1,k} \\ = C_{d_{i+\frac{1}{2},j,k}} E_x|^{n}_{i+\frac{1}{2},j,k} \\ + C_{e_{i+\frac{1}{2},j,k}} H_z|^{n}_{i+\frac{1}{2},j+\frac{1}{2},k} - C_{f_{i+\frac{1}{2},j,k}} H_z|^{n}_{i+\frac{1}{2},j-\frac{1}{2},k} \\ - C_{g_{i+\frac{1}{2},j,k}} \left(H_y|^{n}_{i+\frac{1}{2},j,k+\frac{1}{2}} - H_y|^{n}_{i+\frac{1}{2},j,k-\frac{1}{2}} \right) \\ - C_{h_{i+\frac{1}{2},j,k}} \left(E_y|^{n}_{i+1,j+\frac{1}{2},k} - E_y|^{n}_{i,j+\frac{1}{2},k} \right) \\ + C_{i_{i+\frac{1}{2},j,k}} \left(E_y|^{n}_{i+1,j-\frac{1}{2},k} - E_y|^{n}_{i,j-\frac{1}{2},k} \right) \end{aligned} \quad (11)$$

where

$$C_{a_{i+\frac{1}{2},j,k}} = \left[\begin{array}{c} 1 + \frac{\alpha_{i+\frac{1}{2},j,k}(2\Delta t)^2}{(\Delta y)^2(4\mu_{i+\frac{1}{2},j+\frac{1}{2},k} + \sigma^{\star}_{i+\frac{1}{2},j+\frac{1}{2},k}\Delta t)} \\ + \frac{\alpha_{i+\frac{1}{2},j,k}(2\Delta t)^2}{(\Delta y)^2(4\mu_{i+\frac{1}{2},j-\frac{1}{2},k} + \sigma^{\star}_{i+\frac{1}{2},j-\frac{1}{2},k}\Delta t)} \end{array} \right]$$

$$C_{b_{i+\frac{1}{2},j,k}} = \left[\frac{\alpha_{i+\frac{1}{2},j,k}(2\Delta t)^2}{(\Delta y)^2(4\mu_{i+\frac{1}{2},j+\frac{1}{2},k} + \sigma^{\star}_{i+\frac{1}{2},j+\frac{1}{2},k}\Delta t)} \right]$$

$$C_{c_{i+\frac{1}{2},j,k}} = \left[\frac{\alpha_{i+\frac{1}{2},j,k}(2\Delta t)^2}{(\Delta y)^2(4\mu_{i+\frac{1}{2},j-\frac{1}{2},k} + \sigma^{\star}_{i+\frac{1}{2},j-\frac{1}{2},k}\Delta t)} \right]$$

$$C_{d_{i+\frac{1}{2},j,k}} = \alpha_{i+\frac{1}{2},j,k} \left(4\varepsilon_{i+\frac{1}{2},j,k} - \sigma_{i+\frac{1}{2},j,k}\Delta t \right)$$

$$C_{e_{i+\frac{1}{2},j,k}} = \left[\frac{2\alpha_{i+\frac{1}{2},j,k}\Delta t(4\mu_{i+\frac{1}{2},j+\frac{1}{2},k} - \sigma^{\star}_{i+\frac{1}{2},j+\frac{1}{2},k}\Delta t)}{\Delta y(4\mu_{i+\frac{1}{2},j+\frac{1}{2},k} + \sigma^{\star}_{i+\frac{1}{2},j+\frac{1}{2},k}\Delta t)} \right]$$

$$C_{f_{i+\frac{1}{2},j,k}} = \left[\frac{2\alpha_{i+\frac{1}{2},j,k}\Delta t(4\mu_{i+\frac{1}{2},j-\frac{1}{2},k} - \sigma^{\star}_{i+\frac{1}{2},j-\frac{1}{2},k}\Delta t)}{\Delta y(4\mu_{i+\frac{1}{2},j-\frac{1}{2},k} + \sigma^{\star}_{i+\frac{1}{2},j-\frac{1}{2},k}\Delta t)} \right]$$

$$C_{g_{i+\frac{1}{2},j,k}} = \left[\frac{2\alpha_{i+\frac{1}{2},j,k}\Delta t}{\Delta z(4\varepsilon_{i+\frac{1}{2},j,k} + \sigma_{i+\frac{1}{2},j,k}\Delta t)} \right]$$

$$C_{h_{i+\frac{1}{2},j,k}} = \left[\frac{\alpha_{i+\frac{1}{2},j,k}(2\Delta t)^2}{\Delta x\Delta y(4\mu_{i+\frac{1}{2},j+\frac{1}{2},k} + \sigma^{\star}_{i+\frac{1}{2},j+\frac{1}{2},k}\Delta t)} \right]$$

$$C_{i_{i+\frac{1}{2},j,k}} = \left[\frac{\alpha_{i+\frac{1}{2},j,k}(2\Delta t)^2}{\Delta x\Delta y(4\mu_{i+\frac{1}{2},j-\frac{1}{2},k} + \sigma^{\star}_{i+\frac{1}{2},j-\frac{1}{2},k}\Delta t)} \right]$$

and

$$\alpha_{i+\frac{1}{2},j,k} = \frac{1}{4\varepsilon_{i+\frac{1}{2},j,k} + \sigma_{y_{i+\frac{1}{2},j,k}}\Delta t}$$

We see that Eq. (11) yields a set of simultaneous equations for $E_x|^{n+1/2}$ when written for each j coordinate along a *y-directed* line through the space lattice. The matrix associated with this system is tridiagonal, and hence, easily solved. This process is repeated for each *y-cut* through the grid where E_x components are located.

Similarly, applying steps 1-3 to Eq. (2) and Eq. (4) yields a tridiagonal matrix system for each *z-cut* through the lattice to obtain $E_y|^{n+1/2}$. Applying these steps to Eq. (3) and Eq. (5) yields a tridiagonal matrix system for each *x-cut* through the lattice to obtain $E_z|^{n+1/2}$. Referring back to Fig. 2, we see that these three implicit updating expressions are used during the first half of sub-iteration 1.

Upon evaluating the electric field components everywhere in the grid, we can proceed to the second half of sub-iteration 1, which involves evaluating the magnetic fields. The magnetic field updating equations become fully explicit, as illustrated for $H_z^{n+1/2}$ by rearranging Eq. (10) as follows:

$$\begin{aligned} H_z|^{n+1/2}_{i+\frac{1}{2},j+\frac{1}{2},k} = D_{a_{i+\frac{1}{2},j+\frac{1}{2},k}} H_z|^{n}_{i+\frac{1}{2},j+\frac{1}{2},k} \\ + D_{b_{i+\frac{1}{2},j+\frac{1}{2},k}} \left(\begin{array}{c} \frac{E_x|^{n+1/2}_{i+\frac{1}{2},j+1,k} - E_x|^{n+1/2}_{i+\frac{1}{2},j,k}}{\Delta y} \\ - \frac{E_y|^{n}_{i+1,j+\frac{1}{2},k} - E_y|^{n}_{i,j+\frac{1}{2},k}}{\Delta x} \end{array} \right) \end{aligned} \quad (12)$$

where

$$D_{a_{i+\frac{1}{2},j+\frac{1}{2},k}} = \left(1 - \frac{\sigma^{\star}_{i+\frac{1}{2},j+\frac{1}{2},k}\Delta t}{4\mu_{i+\frac{1}{2},j+\frac{1}{2},k}} \right) \Bigg/ \left(1 + \frac{\sigma^{\star}_{i+\frac{1}{2},j+\frac{1}{2},k}\Delta t}{4\mu_{i+\frac{1}{2},j+\frac{1}{2},k}} \right)$$

$$D_{b_{i+\frac{1}{2},j+\frac{1}{2},k}} = \left(\frac{\Delta t}{2\mu_{i+\frac{1}{2},j+\frac{1}{2},k}} \right) \Bigg/ \left(1 + \frac{\sigma^{\star}_{i+\frac{1}{2},j+\frac{1}{2},k}\Delta t}{4\mu_{i+\frac{1}{2},j+\frac{1}{2},k}} \right)$$

All of the required electric-field component data at time step $n+1/2$ are available upon solving the tridiagonal matrix systems in the manner described above.

B. *Sub-Iteration 2: Advance the 6 field components from time step $n+\frac{1}{2}$ to $n+1$*

Step 1. Again, we start by applying central difference to Eq. 1, only now every term is discretized using finite differences centered at $n+3/4$ as follows:

$$\sigma E_x|^{n+3/4} + \varepsilon \frac{\partial E_x}{\partial t}\Bigg|^{n+3/4} = \frac{\partial H_z}{\partial y}\Bigg|^{n+1/2} - \frac{\partial H_y}{\partial z}\Bigg|^{n+1} \quad (13)$$

Here, the magnetic-field terms are discretized at time steps $n+1/2$ and $n+1$, giving an overall center point of $n+3/4$. Upon substituting centered finite-difference approximations, we obtain the following expression:

$$\begin{aligned} \varepsilon_{i+\frac{1}{2},j,k} \left(\frac{E_x|^{n+1}_{i+\frac{1}{2},j,k} - E_x|^{n+1/2}_{i+\frac{1}{2},j,k}}{\Delta t/2} \right) \\ + \quad \sigma_{i+\frac{1}{2},j,k} \left(\frac{E_x|^{n+1}_{i+\frac{1}{2},j,k} + E_x|^{n+1/2}_{i+\frac{1}{2},j,k}}{2} \right) \\ = \frac{H_z|^{n+1/2}_{i+\frac{1}{2},j+\frac{1}{2},k} - H_z|^{n+1/2}_{i+\frac{1}{2},j-\frac{1}{2},k}}{\Delta y} - \frac{H_y|^{n+1}_{i+\frac{1}{2},j,k+\frac{1}{2}} - H_y|^{n+1}_{i+\frac{1}{2},j,k-\frac{1}{2}}}{\Delta z} \end{aligned} \quad (14)$$

Here, all the fields at time step $n+\frac{1}{2}$ are known; the fields at time step $n+1$ are unknown. Note that for sub-iteration 2, it is now the $\partial H_z/\partial y$ term that is evaluated explicitly from known field data at time step $n+1/2$, while the $\partial H_y/\partial z$ term is evaluated with as-yet unknown field data at time-step $n+1$. Hence, the direction in which the implicit evaluation is used alternates between each sub-iteration.

Step 2. Our aim is to find the value of the unknown E_x at time step $n+1$. However, there are unknown values of H_y on the right hand side of the equation. To eliminate the unknown terms, we apply finite-difference approximations centered at $n+3/4$ to Eq. (5) to obtain the following expression:

$$\begin{aligned}
& \mu_{i+\frac{1}{2},j,k+\frac{1}{2}} \left(\frac{H_y|^{n+1}_{i+\frac{1}{2},j,k+\frac{1}{2}} - H_y|^{n+1/2}_{i+\frac{1}{2},j,k+\frac{1}{2}}}{\Delta t/2} \right) \\
+ \quad & \sigma^{\star}_{i+\frac{1}{2},j,k+\frac{1}{2}} \left(\frac{H_y|^{n+1}_{i+\frac{1}{2},j,k+\frac{1}{2}} + H_y|^{n+1/2}_{i+\frac{1}{2},j,k+\frac{1}{2}}}{2} \right) \\
= \quad & \frac{E_z|^{n+1/2}_{i+1,j,k+\frac{1}{2}} - E_z|^{n+1/2}_{i,j,k+\frac{1}{2}}}{\Delta x} - \frac{E_x|^{n+1}_{i+\frac{1}{2},j,k+1} - E_x|^{n+1}_{i+\frac{1}{2},j,k}}{\Delta z} \qquad (15)
\end{aligned}$$

The two unknowns in this equation are also E_x and H_y at time step $n+1$.

Step 3. Finally, we use Eq. (15) to eliminate the unknown $H_y|^{n+1}$ terms in Eq. (14) and obtain the following expression for the unknown E_x fields at the $n+1^{th}$ time step:

$$\begin{aligned}
\tilde{C}_{a_{i+\frac{1}{2},j,k}} E_x|^{n+1}_{i+\frac{1}{2},j,k} - \tilde{C}_{b_{i+\frac{1}{2},j,k}} E_x|^{n+1}_{i+\frac{1}{2},j,k+1} - \tilde{C}_{c_{i+\frac{1}{2},j,k}} E_x|^{n+1}_{i+\frac{1}{2},j,k-1} & \\
= \tilde{C}_{d_{i+\frac{1}{2},j,k}} E_x|^{n+1/2}_{i+\frac{1}{2},j,k} & \\
- \tilde{C}_{e_{i+\frac{1}{2},j,k}} H_y|^{n+1/2}_{i+\frac{1}{2},j,k+\frac{1}{2}} + \tilde{C}_{f_{i+\frac{1}{2},j,k}} H_y|^{n+1/2}_{i+\frac{1}{2},j,k-\frac{1}{2}} & \\
+ \tilde{C}_{g_{i+\frac{1}{2},j,k}} \left(H_z|^{n+1/2}_{i+\frac{1}{2},j+\frac{1}{2},k} - H_z|^{n+1/2}_{i+\frac{1}{2},j-\frac{1}{2},k} \right) & \\
- \tilde{C}_{h_{i+\frac{1}{2},j,k}} \left(E_z|^{n+1/2}_{i+1,j,k+\frac{1}{2}} - E_z|^{n+1/2}_{i,j,k+\frac{1}{2}} \right) & \\
+ \tilde{C}_{i_{i+\frac{1}{2},j,k}} \left(E_z|^{n+1/2}_{i+1,j,k-\frac{1}{2}} - E_z|^{n+1/2}_{i,j,k-\frac{1}{2}} \right) \qquad (16) &
\end{aligned}$$

where

$$\begin{aligned}
\tilde{C}_{a_{i+\frac{1}{2},j,k}} &= \left[1 + \frac{\alpha_{i+\frac{1}{2},j,k}(2\Delta t)^2}{(\Delta z)^2(4\mu_{i+\frac{1}{2},j,k+\frac{1}{2}} + \sigma^{\star}_{i+\frac{1}{2},j,k+\frac{1}{2}}\Delta t)} + \frac{\alpha_{i+\frac{1}{2},j,k}(2\Delta t)^2}{(\Delta z)^2(4\mu_{i+\frac{1}{2},j,k-\frac{1}{2}} + \sigma^{\star}_{i+\frac{1}{2},j,k-\frac{1}{2}}\Delta t)} \right] \\
\tilde{C}_{b_{i+\frac{1}{2},j,k}} &= \left[\frac{\alpha_{i+\frac{1}{2},j,k}(2\Delta t)^2}{(\Delta z)^2(4\mu_{i+\frac{1}{2},j,k+\frac{1}{2}} + \sigma^{\star}_{i+\frac{1}{2},j,k+\frac{1}{2}}\Delta t)} \right] \\
\tilde{C}_{c_{i+\frac{1}{2},j,k}} &= \left[\frac{\alpha_{i+\frac{1}{2},j,k}(2\Delta t)^2}{(\Delta z)^2(4\mu_{i+\frac{1}{2},j,k-\frac{1}{2}} + \sigma^{\star}_{i+\frac{1}{2},j,k-\frac{1}{2}}\Delta t)} \right] \\
\tilde{C}_{d_{i+\frac{1}{2},j,k}} &= \alpha_{i+\frac{1}{2},j,k} \left(4\varepsilon_{i+\frac{1}{2},j,k} - \sigma_{i+\frac{1}{2},j,k}\Delta t \right) \\
\tilde{C}_{e_{i+\frac{1}{2},j,k}} &= \left[\frac{2\alpha_{i+\frac{1}{2},j,k}\Delta t(4\mu_{i+\frac{1}{2},j,k+\frac{1}{2}} - \sigma^{\star}_{i+\frac{1}{2},j,k+\frac{1}{2}}\Delta t)}{\Delta z(4\mu_{i+\frac{1}{2},j,k+\frac{1}{2}} + \sigma^{\star}_{i+\frac{1}{2},j,k+\frac{1}{2}}\Delta t)} \right] \\
\tilde{C}_{f_{i+\frac{1}{2},j,k}} &= \left[\frac{2\alpha_{i+\frac{1}{2},j,k}\Delta t(4\mu_{i+\frac{1}{2},j,k-\frac{1}{2}} - \sigma^{\star}_{i+\frac{1}{2},j,k-\frac{1}{2}}\Delta t)}{\Delta z(4\mu_{i+\frac{1}{2},j,k-\frac{1}{2}} + \sigma^{\star}_{i+\frac{1}{2},j,k-\frac{1}{2}}\Delta t)} \right] \\
\tilde{C}_{g_{i+\frac{1}{2},j,k}} &= \left[\frac{2\alpha_{i+\frac{1}{2},j,k}\Delta t}{\Delta y(4\varepsilon_{i+\frac{1}{2},j,k} + \sigma_{i+\frac{1}{2},j,k}\Delta t)} \right] \\
\tilde{C}_{h_{i+\frac{1}{2},j,k}} &= \left[\frac{\alpha_{i+\frac{1}{2},j,k}(2\Delta t)^2}{\Delta x\Delta z(4\mu_{i+\frac{1}{2},j,k+\frac{1}{2}} + \sigma^{\star}_{i+\frac{1}{2},j,k+\frac{1}{2}}\Delta t)} \right] \\
\tilde{C}_{i_{i+\frac{1}{2},j,k}} &= \left[\frac{\alpha_{i+\frac{1}{2},j,k}(2\Delta t)^2}{\Delta x\Delta z(4\mu_{i+\frac{1}{2},j,k-\frac{1}{2}} + \sigma^{\star}_{i+\frac{1}{2},j,k-\frac{1}{2}}\Delta t)} \right]
\end{aligned}$$

and

$$\alpha_{i+\frac{1}{2},j,k} = \frac{1}{4\varepsilon_{i+\frac{1}{2},j,k} + \sigma_{y_{i+\frac{1}{2},j,k}}\Delta t}$$

Here, we obtain a tridiagonal matrix system for each *z-cut* through the grid.

Similarly, applying steps 1-3 to Eq. (2) and Eq. (6) yields a tridiagonal matrix system for each *x-cut* through the lattice to obtain $E_y|^{n+1}$. Applying these steps to Eq. (3) and Eq. (4) yields a tridiagonal matrix system for each *y-cut* through the lattice to obtain $E_z|^{n+1}$. Referring back to Fig. 2, we see that these three implicit updating expressions are used during the first half of sub-iteration 2.

Upon evaluating the electric field components everywhere in the grid, we can proceed to the second half of sub-iteration 2, which involves evaluating the magnetic fields. Just as in sub-iteration 1, the magnetic field updating equations become fully explicit, as illustrated for $H_y|^{n+1}$ by rearranging Eq. (15) as follows:

$$\begin{aligned}
H_y|^{n+1}_{i+\frac{1}{2},j,k+\frac{1}{2}} = & \tilde{D}_{a_{i+\frac{1}{2},j,k+\frac{1}{2}}} H_y|^{n+1/2}_{i+\frac{1}{2},j,k+\frac{1}{2}} \\
& + \tilde{D}_{b_{i+\frac{1}{2},j,k+\frac{1}{2}}} \begin{pmatrix} \frac{E_z|^{n+1/2}_{i+1,j,k+\frac{1}{2}} - E_z|^{n+1/2}_{i,j,k+\frac{1}{2}}}{\Delta x} \\ -\frac{E_x|^{n+1}_{i+\frac{1}{2},j,k+1} - E_x|^{n+1}_{i+\frac{1}{2},j,k}}{\Delta z} \end{pmatrix} \qquad (17)
\end{aligned}$$

where

$$\begin{aligned}
\tilde{D}_{a_{i+\frac{1}{2},j,k+\frac{1}{2}}} &= \left(1 - \frac{\sigma^{\star}_{i+\frac{1}{2},j,k+\frac{1}{2}}\Delta t}{4\mu_{i+\frac{1}{2},j,k+\frac{1}{2}}} \right) \Bigg/ \left(1 + \frac{\sigma^{\star}_{i+\frac{1}{2},j,k+\frac{1}{2}}\Delta t}{4\mu_{i+\frac{1}{2},j,k+\frac{1}{2}}} \right) \\
\tilde{D}_{b_{i+\frac{1}{2},j,k+\frac{1}{2}}} &= \left(\frac{\Delta t}{2\mu_{i+\frac{1}{2},j,k+\frac{1}{2}}} \right) \Bigg/ \left(1 + \frac{\sigma^{\star}_{i+\frac{1}{2},j,k+\frac{1}{2}}\Delta t}{4\mu_{i+\frac{1}{2},j,k+\frac{1}{2}}} \right)
\end{aligned}$$

All of the required electric-field component data at time step $n+1$ are available upon solving the tridiagonal matrix systems in the manner described above. This completes the algorithm.

IV. **Numerical Formulation for the FDTD-ADI Algorithm with PML ABCs**

Upon applying the formulation presented in Section III to the split-field version of Maxwell's equations:

$$\varepsilon\frac{\partial E_{x_y}}{\partial t}+\sigma_y E_{x_y}=\frac{\partial H_z}{\partial y} \quad \varepsilon\frac{\partial E_{x_z}}{\partial t}+\sigma_z E_{x_z}=-\frac{\partial H_y}{\partial z} \tag{18}$$

$$\varepsilon\frac{\partial E_{y_z}}{\partial t}+\sigma_z E_{y_z}=\frac{\partial H_x}{\partial z} \quad \varepsilon\frac{\partial E_{y_x}}{\partial t}+\sigma_x E_{y_x}=-\frac{\partial H_z}{\partial x} \tag{19}$$

$$\varepsilon\frac{\partial E_{z_x}}{\partial t}+\sigma_x E_{z_x}=\frac{\partial H_y}{\partial x} \quad \varepsilon\frac{\partial E_{z_y}}{\partial t}+\sigma_y E_{z_y}=-\frac{\partial H_x}{\partial y} \tag{20}$$

$$\mu\frac{\partial H_{x_y}}{\partial t}+\sigma_y^\star H_{x_y}=-\frac{\partial E_z}{\partial y} \quad \mu\frac{\partial H_{x_z}}{\partial t}+\sigma_z^\star H_{x_z}=\frac{\partial E_y}{\partial z} \tag{21}$$

$$\mu\frac{\partial H_{y_z}}{\partial t}+\sigma_z^\star H_{y_z}=-\frac{\partial E_x}{\partial z} \quad \mu\frac{\partial H_{y_x}}{\partial t}+\sigma_x^\star H_{y_x}=\frac{\partial E_z}{\partial x} \tag{22}$$

$$\mu\frac{\partial H_{z_x}}{\partial t}+\sigma_x^\star H_{z_x}=-\frac{\partial E_y}{\partial x} \quad \mu\frac{\partial H_{z_y}}{\partial t}+\sigma_y^\star H_{z_y}=\frac{\partial E_x}{\partial y}, \tag{23}$$

we obtain an FDTD-ADI formulation for PML ABCs[1]. The derivation is very similar to that described in the previous section, and therefore the steps are not repeated here. Instead, we present only the resulting finite-difference expressions for the E_x, H_y, and H_z field components for comparison with the corresponding expressions presented in Section III.

A. Sub-Iteration 1: Advance the 12 split-field components from time step n to time step n + 1/2

Steps 1-3 applied to the split-field equations for E_x and H_z (Eq. (18) and Eq. (23)), yield an explicit finite-difference expression for the unknown E_{x_z} fields at the $n+\frac{1}{2}^{th}$ time step:

$$\begin{aligned} E_{x_z}\big|^{n+1/2}_{i+\frac{1}{2},j,k} &= C_{aa_{i+\frac{1}{2},j,k}}\, E_{x_z}\big|^{n}_{i+\frac{1}{2},j,k} \\ &\quad - C_{bb_{i+\frac{1}{2},j,k}}\left(\begin{array}{c} \frac{H_{y_z}\big|^n_{i+\frac{1}{2},j,k+\frac{1}{2}}-H_{y_z}\big|^n_{i+\frac{1}{2},j,k-\frac{1}{2}}}{\Delta z} \\ +\frac{H_{y_x}\big|^n_{i+\frac{1}{2},j,k+\frac{1}{2}}-H_{y_x}\big|^n_{i+\frac{1}{2},j,k-\frac{1}{2}}}{\Delta z}\end{array}\right) \end{aligned} \tag{24}$$

where,

$$C_{aa_{i+\frac{1}{2},j,k}} = \left[\frac{1-\frac{\sigma_{z_{i+\frac{1}{2},j,k}}\Delta t}{4\varepsilon_{i+\frac{1}{2},j,k}}}{1+\frac{\sigma_{z_{i+\frac{1}{2},j,k}}\Delta t}{4\varepsilon_{i+\frac{1}{2},j,k}}}\right]$$

$$C_{bb_{i+\frac{1}{2},j,k}} = \left[\frac{\frac{\Delta t}{2\varepsilon_{i+\frac{1}{2},j,k}}}{1+\frac{\sigma_{z_{i+\frac{1}{2},j,k}}\Delta t}{4\varepsilon_{i+\frac{1}{2},j,k}}}\right]$$

[1]We note that a recent publication by Liu and Gedney also reports an FDTD-ADI formulation for PML ABCs[15]. Our work was developed independently from theirs, and submitted for publication simultaneously.

and an implicit finite-difference expression for the unknown E_{x_y} fields at the $n+\frac{1}{2}^{th}$ time step:

$$\begin{aligned} & C_{a_{i+\frac{1}{2},j,k}} E_{x_y}\Big|^{n+1/2}_{i+\frac{1}{2},j,k} - C_{b_{i+\frac{1}{2},j,k}} E_{x_y}\Big|^{n+1/2}_{i+\frac{1}{2},j+1,k} \\ & - C_{c_{i+\frac{1}{2},j,k}} E_{x_y}\Big|^{n+1/2}_{i+\frac{1}{2},j-1,k} \\ = \;& C_{d_{i+\frac{1}{2},j,k}}\, E_{x_y}\big|^n_{i+\frac{1}{2},j,k} + C_{e_{y_{i+\frac{1}{2},j,k}}} H_{z_y}\big|^n_{i+\frac{1}{2},j+\frac{1}{2},k} \\ & - C_{f_{y_{i+\frac{1}{2},j,k}}} H_{z_y}\big|^n_{i+\frac{1}{2},j-\frac{1}{2},k} + C_{e_{x_{i+\frac{1}{2},j,k}}} H_{z_x}\big|^n_{i+\frac{1}{2},j+\frac{1}{2},k} \\ & - C_{f_{x_{i+\frac{1}{2},j,k}}} H_{z_x}\big|^n_{i+\frac{1}{2},j-\frac{1}{2},k} - C_{g_{i+\frac{1}{2},j,k}}\left(\begin{array}{c} E_{y_x}\big|^n_{i+1,j+\frac{1}{2},k} \\ -E_{y_x}\big|^n_{i,j+\frac{1}{2},k}\end{array}\right) \\ & + C_{h_{i+\frac{1}{2},j,k}}\left(\begin{array}{c} E_{y_x}\big|^n_{i+1,j-\frac{1}{2},k} \\ -E_{y_x}\big|^n_{i,j-\frac{1}{2},k}\end{array}\right) - C_{g_{i+\frac{1}{2},j,k}}\left(\begin{array}{c} E_{y_z}\big|^n_{i+1,j+\frac{1}{2},k} \\ -E_{y_z}\big|^n_{i,j+\frac{1}{2},k}\end{array}\right) \\ & + C_{h_{i+\frac{1}{2},j,k}}\left(\begin{array}{c} E_{y_z}\big|^n_{i+1,j-\frac{1}{2},k} \\ -E_{y_z}\big|^n_{i,j-\frac{1}{2},k}\end{array}\right) + C_{i_{i+\frac{1}{2},j,k}}\left(\begin{array}{c} E_{x_z}\big|^{n+1/2}_{i+\frac{1}{2},j+1,k} \\ -E_{x_z}\big|^{n+1/2}_{i+\frac{1}{2},j,k}\end{array}\right) \\ & - C_{j_{i+\frac{1}{2},j,k}}\left(\begin{array}{c} E_{x_z}\big|^{n+1/2}_{i+\frac{1}{2},j,k} \\ -E_{x_z}\big|^{n+1/2}_{i+\frac{1}{2},j-1,k}\end{array}\right) \end{aligned} \tag{25}$$

where

$$C_{a_{i+\frac{1}{2},j,k}} = \left[\begin{array}{c} 1+\frac{\alpha_{i+\frac{1}{2},j,k}(2\Delta t)^2}{(\Delta y)^2(4\mu_{i+\frac{1}{2},j+\frac{1}{2},k}+\sigma^\star_{y_{i+\frac{1}{2},j+\frac{1}{2},k}}\Delta t)} \\ +\frac{\alpha_{i+\frac{1}{2},j,k}(2\Delta t)^2}{(\Delta y)^2(4\mu_{i+\frac{1}{2},j-\frac{1}{2},k}+\sigma^\star_{y_{i+\frac{1}{2},j-\frac{1}{2},k}}\Delta t)}\end{array}\right]$$

$$C_{b_{i+\frac{1}{2},j,k}} = \left[\frac{\alpha_{i+\frac{1}{2},j,k}(2\Delta t)^2}{(\Delta y)^2(4\mu_{i+\frac{1}{2},j+\frac{1}{2},k}+\sigma^\star_{y_{i+\frac{1}{2},j+\frac{1}{2},k}}\Delta t)}\right]$$

$$C_{c_{i+\frac{1}{2},j,k}} = \left[\frac{\alpha_{i+\frac{1}{2},j,k}(2\Delta t)^2}{(\Delta y)^2(4\mu_{i+\frac{1}{2},j-\frac{1}{2},k}+\sigma^\star_{y_{i+\frac{1}{2},j-\frac{1}{2},k}}\Delta t)}\right]$$

$$C_{d_{i+\frac{1}{2},j,k}} = \alpha_{i+\frac{1}{2},j,k}\left(4\varepsilon_{i+\frac{1}{2},j,k}-\sigma_{y_{i+\frac{1}{2},j,k}}\Delta t\right)$$

$$C_{e_{u_{i+\frac{1}{2},j,k}}} = \left[\frac{2\alpha_{i+\frac{1}{2},j,k}\Delta t(4\mu_{i+\frac{1}{2},j+\frac{1}{2},k}-\sigma^\star_{u_{i+\frac{1}{2},j+\frac{1}{2},k}}\Delta t)}{\Delta y(4\mu_{i+\frac{1}{2},j+\frac{1}{2},k}+\sigma^\star_{u_{i+\frac{1}{2},j+\frac{1}{2},k}}\Delta t)}\right]$$

$$C_{f_{u_{i+\frac{1}{2},j,k}}} = \left[\frac{2\alpha_{i+\frac{1}{2},j,k}\Delta t(4\mu_{i+\frac{1}{2},j-\frac{1}{2},k}-\sigma^\star_{u_{i+\frac{1}{2},j-\frac{1}{2},k}}\Delta t)}{\Delta y(4\mu_{i+\frac{1}{2},j-\frac{1}{2},k}+\sigma^\star_{u_{i+\frac{1}{2},j-\frac{1}{2},k}}\Delta t)}\right]$$

$$C_{g_{i+\frac{1}{2},j,k}} = \left[\frac{\alpha_{i+\frac{1}{2},j,k}(2\Delta t)^2}{\Delta x\Delta y(4\mu_{i+\frac{1}{2},j+\frac{1}{2},k}+\sigma^\star_{x_{i+\frac{1}{2},j+\frac{1}{2},k}}\Delta t)}\right]$$

$$C_{h_{i+\frac{1}{2},j,k}} = \left[\frac{\alpha_{i+\frac{1}{2},j,k}(2\Delta t)^2}{\Delta x\Delta y(4\mu_{i+\frac{1}{2},j-\frac{1}{2},k}+\sigma^\star_{x_{i+\frac{1}{2},j-\frac{1}{2},k}}\Delta t)}\right]$$

$$C_{i_{i+\frac{1}{2},j,k}} = \left[\frac{\alpha_{i+\frac{1}{2},j,k}(2\Delta t)^2}{\Delta y^2(4\mu_{i+\frac{1}{2},j+\frac{1}{2},k}+\sigma^{\star}_{y_{i+\frac{1}{2},j+\frac{1}{2},k}}\Delta t)}\right]$$

$$C_{j_{i+\frac{1}{2},j,k}} = \left[\frac{\alpha_{i+\frac{1}{2},j,k}(2\Delta t)^2}{\Delta y^2(4\mu_{i+\frac{1}{2},j-\frac{1}{2},k}+\sigma^{\star}_{y_{i+\frac{1}{2},j-\frac{1}{2},k}}\Delta t)}\right]$$

and

$$\alpha_{i+\frac{1}{2},j,k} = \frac{1}{4\varepsilon_{i+\frac{1}{2},j,k}+\sigma_{y_{i+\frac{1}{2},j,k}}\Delta t} \tag{26}$$

Note that the implicit update of E_{x_y} is similar to the implicit update of E_x in the non-PML formulation of Section III wherein a tridiagonal matrix system is solved for *y-cuts* through the grid. The first half of sub-iteration 1 continues in a similar manner with an explicit update of E_{y_x}, an implicit update of E_{y_z} for *z-cuts* through the grid, an explicit update of E_{z_y}, and an implicit update of E_{z_x} for *x-cuts* through the grid.

The second half of sub-iteration 1 involves evaluating the magnetic fields using fully explicit finite-difference expressions, as illustrated by the following expressions for H_{z_x} and H_{z_y}:

$$H_{z_x}\big|^{n+1/2}_{i+\frac{1}{2},j+\frac{1}{2},k} = Da_{x_{i+\frac{1}{2},j,k+\frac{1}{2}}}\, H_{z_x}\big|^{n}_{i+\frac{1}{2},j+\frac{1}{2},k} + Db_{x_{i+\frac{1}{2},j,k+\frac{1}{2}}}\left(\begin{array}{l}\dfrac{E_{y_x}\big|^{n}_{i+1,j+\frac{1}{2},k}-E_{y_x}\big|^{n}_{i,j+\frac{1}{2},k}}{\Delta x}\\ +\dfrac{E_{y_z}\big|^{n}_{i+1,j+\frac{1}{2},k}-E_{y_z}\big|^{n}_{i,j+\frac{1}{2},k}}{\Delta x}\end{array}\right) \tag{27}$$

$$H_{z_y}\big|^{n+1/2}_{i+\frac{1}{2},j+\frac{1}{2},k} = Da_{y_{i+\frac{1}{2},j,k+\frac{1}{2}}}\, H_{z_y}\big|^{n}_{i+\frac{1}{2},j+\frac{1}{2},k} + Db_{y_{i+\frac{1}{2},j,k+\frac{1}{2}}}\left(\begin{array}{l}\dfrac{E_{x_y}\big|^{n+1/2}_{i+\frac{1}{2},j+1,k}-E_{x_y}\big|^{n+1/2}_{i+\frac{1}{2},j,k}}{\Delta y}\\ +\dfrac{E_{x_z}\big|^{n+1/2}_{i+\frac{1}{2},j+1,k}-E_{x_z}\big|^{n+1/2}_{i+\frac{1}{2},j,k}}{\Delta y}\end{array}\right) \tag{28}$$

where

$$D_{a_{u_{i+\frac{1}{2},j,k+\frac{1}{2}}}} = \left(1-\frac{\sigma^{\star}_{u_{i+\frac{1}{2},j+\frac{1}{2},k}}\Delta t}{4\mu_{i+\frac{1}{2},j+\frac{1}{2},k}}\right)\Bigg/\left(1+\frac{\sigma^{\star}_{u_{i+\frac{1}{2},j+\frac{1}{2},k}}\Delta t}{4\mu_{i+\frac{1}{2},j+\frac{1}{2},k}}\right) \tag{29}$$

$$D_{b_{u_{i+\frac{1}{2},j,k+\frac{1}{2}}}} = \left(\frac{\Delta t}{2\mu_{i+\frac{1}{2},j+\frac{1}{2},k}}\right)\Bigg/\left(1+\frac{\sigma^{\star}_{u_{i+\frac{1}{2},j+\frac{1}{2},k}}\Delta t}{4\mu_{i+\frac{1}{2},j+\frac{1}{2},k}}\right) \tag{30}$$

B. Sub-Iteration 2: Advance the 12 split-field components from time step $n+\frac{1}{2}$ to time step $n+1$

Similarly, for the first half of sub-iteration 2, the finite-difference expressions to be implemented during sub-iteration 2 involve an explicit update of E_{x_y}, an implicit update of E_{x_z} along *z-cuts* through the grid, an explicit update of E_{y_z}, an implicit update of E_{y_x} for *x-cuts* through the grid, an explicit update of E_{z_x}, and an implicit update of E_{z_y} for *y-cuts* through the grid. The second half of sub-iteration 2 is completed by evaluating the magnetic fields using fully explicit finite-difference expressions. This concludes the algorithm.

V. **Numerical Examples**

To demonstrate the computational efficiency of the generalized FDTD-ADI for relevant VLSI interconnect geometries, we have designed a rigorous test case [2] involving a 5-mm-long microstrip transmission line, as illustrated in Figure 3. The width of the microstrip is 10 μm. Located between the microstrip and the ground plane is a 1-μm-thick low-loss dieletric substrate ($\varepsilon_r = 4.0, \sigma = 0.5\times10^{-3}$ S/m). The region above the microstrip is filled with free space ($\varepsilon_r = 1.0, \sigma = 0.0$). A current source is modeled at one end of the microstrip; the other end is terminated with an open-circuit. The excitation waveform is a baseband Gaussian pulse:

$$J_{z_{\text{source}}} = J_0 e^{-(t-t_0)^2/\tau^2} \tag{31}$$

where $t_0 = 3\tau$ and $\tau = 5$ ps. With this ultrashort pulse, we are able to use the standard FDTD algorithm as a benchmark simulation and the generalized FDTD-ADI algorithm as the test simulation for the same structure. Based on the spectral content of the pulse, we conclude that the minimum wavelength of interest is approximately 2 mm in the dielectric substrate. Therefore, our grid cell size should be no larger than 200 μm. In order to model the thin substrate, we must choose $\Delta z = 1$ μm; for the other spatial increments, we use $\Delta x = 20$ μm and $\Delta y = 5$ μm. Note that since the smallest geometrical feature (the height of the substrate) is much smaller than smallest wavelength of interest, we are in the regime discussed in Section II where the limit on Δt is much smaller than needed for numerical accuracy. For the standard FDTD algorithm, the Courant limit requires that $\Delta t \le 3.26$ fs. Accordingly, the time step in our standard FDTD simulation is chosen to be $\Delta t_{\text{FDTD}} = 3.0$ fs. For the FDTD-ADI algorithm, there is no stability bound on the time step, so we have chosen $\Delta t_{\text{FDTD-ADI}} = 60$ fs; in this case, $\Delta t_{\text{FDTD-ADI}}/\Delta t_{\text{FDTD}} = 20$.

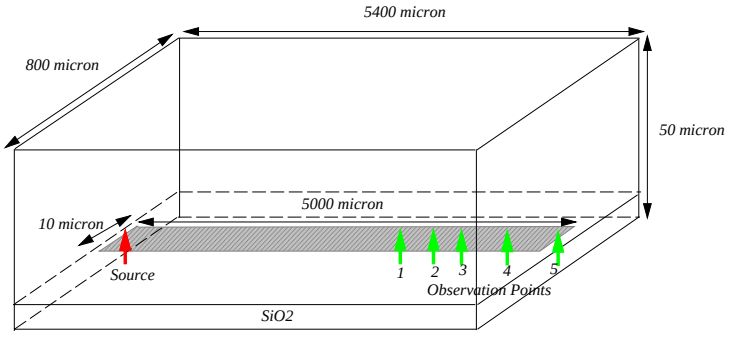

Fig. 3. Microstrip transmission model.

First, we place an observation point 0.5 mm from the source end of the transmission line. For both the standard FDTD and FDTD-ADI models, we record the time history of E_z between the ground plane and the microstrip at this observation point. These temporal waveforms are displayed in Figure 4. The standard FDTD simulation is run for a total of 20,000 time steps (a duration of 60 ps).

[2] We will discuss several additional examples in our presentation; these will also be posted on our web site.

Within this time window, we observe the incident pulse pass our observation point. For the FDTD-ADI case, the same 60-ps simulation requires only 1000 time steps. Therefore, we run the FDTD-ADI simulation for 2000 time steps to show not only the incident pulse, but also the reflected and retro-reflected pulses which overlap in time at our observation point in space. We have normalized both waveforms to the peak of the incident E_z field. There is excellent agreement between the FDTD-computed waveform (solid line) and the FDTD-ADI-computed waveform (dotted line) over the time window in which both data sets are computed.

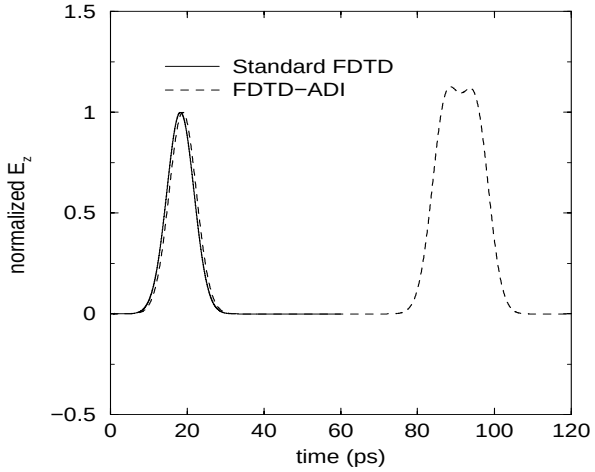

Fig. 4. Normalized E_z field observed 0.5 mm from the source end of the microstrip.

Second, we place five observation points at distances $d = 2.0$, 1.5, 1.0, 0.5, and 0.0 mm from the load end of the transmission line. Here we run only the FDTD-ADI case since a longer length of time is required to observe the pulse reach the load end of the line, 5 mm from the source. Figure 5 shows the FDTD-ADI-computed waveforms observed at these five observation points. The incident and reflected pulses overlap in time to varying degrees depending on the location of the observation point. The results agree with theoretical predictions for time-domain reflections from a line terminated with an open-circuited load.

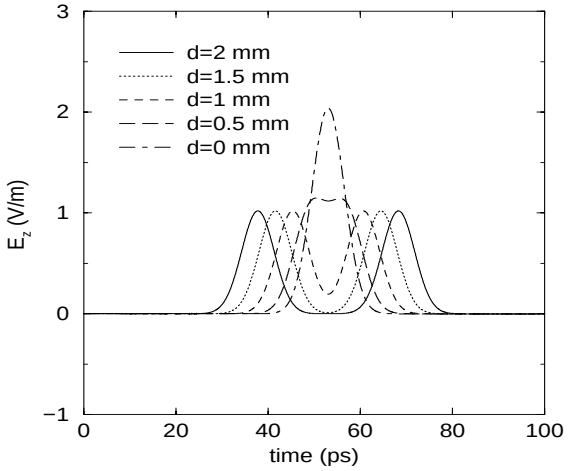

Fig. 5. FDTD-ADI-computed E_z field at five different observation points near the load end of the microstrip.

VI. **Conclusions**

The FDTD-ADI algorithm has significant promise for stable and accurate FDTD modeling of electromagnetic wave phenomena in VLSI interconnects. As demonstrated in this paper, the number of time steps needed to complete the full-wave time-domain simulation can be reduced by an order of magnitude or more.

VII. **Acknowledgements**

The authors would like to thank S. Borkar, T. Karnik, A. Alvandpour, R. Krishnamurth, F. Dartu and N. Menezes from Intel Corp. and R. Szalapski and Y.Z. Liao from Avant! Corp. for helpful discussions.

REFERENCES

[1] K. Nabors and J. White, "Fastcap: a multipole accelerated 3-d capacitance extraction program," *IEEE Trans. on Computer-Aided Design of Integrated Circuits and Systems*, vol. 10, no. 11, 1991.

[2] W. Shi, J. Liu, N. Kakani, and T. Yu, "A fast hierarchical algorithm for 3-d capacitance extraction," in *Design Automation Conference*, 1998.

[3] M. Kamon, M.J. Ttsuk, and J.K. White, "Fasthenry: a multipole-accelerated 3-d inductance extraction program," *IEEE Trans. on Microwave Theory and Techniques*, vol. 42, pp. 1750–1758, Sept. 1994.

[4] J. Cullum, A. Ruehli, and T. Zhang, "A method for reduced-order modeling and simulation of large interconnect circuits and its application to peec models with retardation," *IEEE Trans. on Circuits and Systems II: Analog and Digital Signal Processing*, vol. 47, no. 4, pp. 261–273, 2000.

[5] R. Mittra, W. D. Becker, and P. H. Harms, "A general purpose Maxwell solver for the extraction of equivalent circuits of electronic package components for circuit simulation," *IEEE Trans. on Circuits and Systems I: Fundamental Theory and Applications*, vol. 39, no. 11, pp. 964–973, 1992.

[6] M. Piket-May, A. Taflove, and J. Baron, "FD-TD modeling of digital signal propagation in 3-D circuits with passive and active loads," *IEEE Trans. on Microwave Theory and Techniques*, vol. 42, pp. 1514–1523, Aug. 1994.

[7] P. Vichot, J. A. Mix, Z. Schoenborn, J. Dunn, and M. Piket-May, "Numerical modeling of a clock distribution network for a superconducting multichip module," *IEEE Trans. on Components, Hybrids, and Manufacturing Technology, Part B: Advanced Packaging*, vol. 21, pp. 98–104, Feb. 1998.

[8] Y.-S. Tsuei, A. C. Cangellaris, and J. L. Prince, "Rigorous electromagnetic modeling of chip-to-package (first-level) interconnections," *IEEE Trans. on Components, Hybrids, and Manufacturing Technology*, vol. 16, no. 8, pp. 876–883, 1993.

[9] H. H. M. Ghouz and E.-B. El-Sharawy, "An accurate equivalent circuit model of flip chip and via interconnects," *IEEE Trans. on Microwave Theory and Techniques*, vol. 44, no. 12, pp. 2543–2554, Dec. 1996.

[10] K. L. Shlager and J. B. Schneider, "A survey of the finite-difference time-domain literature," in *Advances in Computational Electrodynamics: The Finite-Difference Time-Domain Method*, A. Taflove, Ed., chapter 1, pp. 1–62. Artech House, Boston, MA, 1998.

[11] T. Namiki, "A new FDTD algorithm based on alternating-direction implicit method," *IEEE Trans. on Microwave Theory and Techniques*, vol. 47, pp. 2003–2007, Oct. 1999.

[12] F. Zheng, Z. Chen, and J. Zhang, "A finite-difference time-domain method without the Courant stability conditions," *IEEE Microwave Guided Wave Letters*, vol. 9, pp. 441–443, Nov. 1999.

[13] J.-P. Berenger, "A perfectly matched layer for the absorption of electromagnetic waves," *J. Computational Physics*, vol. 114, no. 1, pp. 185–200, 1994.

[14] A. Taflove and S. Hagness, *Computational Electrodynamics: The Finite-Difference Time-Domain Method, 2 ed.*, Artech House, Boston, MA, 2000.

[15] G. Liu and S. D. Gedney, "Perfectly matched layer media for an unconditionally stable three-dimensional ADI-FDTD method," *IEEE Microwave Guided Wave Letters*, vol. 10, no. 7, pp. 261–263, 2000.